PCCP
Physical Chemistry Chemical Physics

Accepted Manuscript

This article can be cited before page numbers have been issued, to do this please use: E. M. Gavilán Arriazu, R. E. Giménez and O. A. Pinto, *Phys. Chem. Chem. Phys.*, 2020, DOI: 10.1039/D0CP03348K.

ROYAL SOCIETY OF CHEMISTRY

rsc.li/pccp

View Article Online
DOI: 10.1039/D0CP03348K

Structural surface and thermodynamics analysis of nanoparticles with defects

E.M. Gavilán-Arriazu[1], Rodrigo E. Giménez[2] and O. A. Pinto[1*]

[1]*Instituto de Bionanotecnología del NOA (INBIONATEC-CONICET), Universidad Nacional de Santiago de Estero, RN 9 Km 1125 Villa el Zanjón, Santiago del Estero, G4206XCP, Argentina*

[2]*Laboratorio de Biointerfases y Sistemas Biomiméticos, Centro de Investigaciones en Biofisica Aplicada y Alimentos (CIBAAL) (UNSE-CONICET), Villa el Zanjón, Santiago del Estero, Argentina*

* Corresponding author: oapinto@unsl.edu.ar

Keyword: Monte Carlo simulation; Lattice-gas model, nanoparticles, structural surface .

Abstract

In this work, we analyze the surface structure and the thermodynamics regarding the decorations of nanoparticles with defects, using statistical calculations and Monte Carlo simulations in a complementary way. The main objective is to design and analyze a simple model as a general tool that can help more specific and complex models to interpret their results. In particular, we show how the presence of surface defects of the same nature of the nanoparticle, induce different sites distributions depending on different factors: the density of defects, the geometry and size of the considered nanoparticle. Those distributions are analyzed for an icosahedron nanoparticle of different size and density of defects, and then are linked with Monte Carlo simulations to interpret the thermodynamic effects of the modified surfaces. For low temperature or strong attractive interactions conditions, the details emerging from the defective surfaces were manifested as wide plateaus in the isotherm and peaks in the compressibility of the adlayer. Different situation was observed as temperature rises, since the structural details gradually

disappear from the thermodynamic measurements, until plateaus and compressibility peaks completely merge for high enough temperature conditions. Adsorption sites distribution, adsorption isotherms, energy per site, compressibility of the adlayer, and other relevant properties are analyzed as a function of the number of defects and the chemical potential. In addition to the icosahedron, cuboctahedron and truncated octahedron geometries are also analyzed.

1. Introduction

The superficial defects in the low scale systems have aroused much interest in recent years, in many fields [1,2], because small surface variations can modify the thermodynamic and the structural properties of the entire system. In particular, in small-scale systems, such as nanoparticles [3,4], nanotubes [5], nanoholes, this is more evident. These defects induce energetic and geometric unbalance that modifies the surface structure and favors several surface processes, for example, condensation. In this work, we are interested in nanoparticles (NP) on which atoms or molecules may be deposited. Before the deposition, NPs can be obtained by several methods of synthesis [6-8]. Usually in such procedures, the NPs acquire a certain ordered structure where the surface atoms has properties, different from the crystalline bulk. However, amorphous NP or with defects has its own properties too [9, 10]. In a simple way, defects can be generated by introducing or removing particles on the NP surface [11,12], this modifies the coordination and the energy of atoms. The properties arising from the NP surface modification can show important improvements in comparison with the ordered structure, for example, in catalysis [13], magnetism [14], materials with enhanced bioactivity[15], just to mention a few. Experimental and simulations studies have been focused on improving these properties and others [16-18].

View Article Online
DOI: 10.1039/D0CP03348K

In the last years, many computational and mathematics tools have been used to understand the physicochemical processes that occur in flats surface, even in nanostructures [19-22]. In particular, electrochemical processes have been studied applying various methodologies [23-28]. It is possible to connect the thermodynamics of adsorption with the voltammetric process. The current densities in voltammetric curves can be obtained from the derivative of the adsorption isotherms or by the ad-particles fluctuations [29]. This method has been applied in several experimental systems, such as urea on Pt(100) and bisulfate on Rh(111) by ground-state calculations and Grand canonical Monte Carlo simulation (GCMC) [30]. It was also used in the underpotential deposition of Cu on Au(111) in the presence of sulfate [31] and the electrosorption of Br on Ag(100)[32,33].

The possibility of manipulating parameters gives to modeling and simulation methods certain advantages to study and understand complex systems front of experimental techniques. For example, in the low scale systems, standard Monte Carlo simulation [34-36] and lattice gas model have been an important tool to analyze the thermodynamics of decoration on many systems: nanotubes [37,38], nanoholes [39,40], NPs[41-43].Even other theoretical approximation such as Mean field approaches were used [44].

In the simulations field, several complex models were used to analyze the behavior of nanoparticles with structural defects. Monti et al. [45] have used Molecular Dynamic (MD) simulations and reactive force fields to study the decoration of Cysteine on gold nanoparticles. Using MD too, Hoang et al. have studied the structural properties of different amorphous nanoparticles, with a double-well interaction pair potential [46,47]. Furthermore, other authors have used MD to study the thermal stability, the nucleation and the growth of nanoparticles [48-50]. On the other hand, Monte Carlo (MC)

simulations have demonstrated to be an efficient method to study the structural properties of nanoparticles. For example, Yun et al. [51] performed MC simulations to study the structure of bimetallic nanoparticles with the embedded atom method potential (EAM). In the same way, Tun-Dong et al. [52] have analyzed Pt-Pd nanoparticles stability.

When decorating ordered metallic NPs with adsorbate-NP attractive interactions [53], the isotherms show the formation of several plateaus, which are identified with different filling stages. These plateaus can be associated with the filling of different types of sites on the nanoparticle surface: facets, borders and vertices. Other important characteristic is the evidence of the "*nanoefects*", which are attributed only to the nanoscale. This means that NP size and geometry considerable affects the thermodynamic variables.

Understanding the structural details let construct the energetic topology related to the NP geometry. With this information it is possible to build mathematical models to understand the impact of the structure on the phenomena occurring on NP surfaces, like decoration. So, the main objective of this work is trying to identify and characterize the most prominent features in the low scale for nanoparticles with defects, principally the structural details and the decoration phenomenon on NP surfaces. Hoping that this methodology can serve as a tool or a reference for the elucidation of the results emerging from more specific and complex models, closer to the experimental conditions.

The article is organized as follows: in section 2, Theoretical model and Monte Carlo simulation are presented. The results and discussion are presented in Section 3, divided in Structural surface analysis and Monte Carlo simulations. Finally, the conclusions are draw in Section 4.

2- Theoretical model and Monte Carlo Simulation

View Article Online
DOI: 10.1039/D0CP03348K

Frequently, in labs, NPs are generated with isolated atoms on its surface that may or may not be as same species as the seed. These atoms generate surfaces imperfections or defects, that can be well characterized and studied with simulations, as we will show.

With a lattice gas model, it is possible to mimic the NP seed consisting of N_A atoms with N adsorption sites on its surface. Foreign particles can be deposited then on any of these N sites.

In the present study we consider the case for an icosahedral (ICO) NP, this nanoparticle geometry is used as an example, but similar analyzes can be made with other NPs. In principle, the ICO NP surface can be formed by Mackay or anti-Mackay sites [54-56]. Since the presence of ani-Mackay sites is more important in the case that particles C were of different nature of the seed, and of bigger size, and this is not the case, we consider a NP with Mackay sites only.

With this considerations, in a clean ICO NP, i.e. without surface defects , there are three different kind of sites on its surface: i) facets, where each adatom is linked with three atoms from the seed and six lateral nearest neighbors, ii) Edges sites, where adatoms are linked with two atoms from the seed and six laterals nearest neighbors, iii) Vertices sites, where are linked with just one site of the seed and five lateral nearest neighbors. In short: facets have nine first nearest neighbors, edges have eight and the vertices have six. However, in the present model, a clean NP surface can be modified by the irreversible deposition of external atoms of the same or different nature of the seed. Hence, the surface will be formed by two different kind of atoms: atoms of the seed, and those irreversibly deposited. For simplicity, we will call particles A to all those from the NP seed, particles B for the reversible adsorbed species, and particles C to those irreversible deposited which modifies the NP surface. The C particles will then modify the energy of the sites available for adsorption.

In nanostructured systems, the interaction energy defines the type of approach considered. For example, multibody interaction [57], non-additive lateral interactions [58] and embedded atom method were used to describe nanoparticles [61,62]. However, take into account many-body potentials is expensive from a computational viewpoint. On the other hand, pairwise description is sufficiently accurate because the higher-order energetics terms cancel each other, as it has been observed in reference [61]. With all these considerations, our approach considers additive pairwise interactions.

The energetic can be considered as follow: if a foreign B-particle is deposited, it "fells" different kinds of energies: w_{BA} with A-particles, w_{BC}, with C-particles and w_{BB}. With these considerations, the Hamiltonian can be expressed by

$$H(N) = \frac{1}{2}\sum_{<i,j>}\left(w_{BB}\,\delta_{c_i,-1}\delta_{c_j,-1} + w_{BA}\,\delta_{c_i,-1}\delta_{c_j,1} + w_{BC}\,\delta_{c_i,-1}\delta_{c_j,2}\right) - \mu\sum_{i}^{M} c_i \qquad (1)$$

where c_i is the occupation variable of the i-th site, which takes the value 1 if the site is occupied by A, -1 if occupied by B, 2 if occupied by C, and 0 in any other case. The first and second sums run over all available sites and all first nearest-neighbors (NNs) pairs respectively.

The value of the w_{BC} energy, is useful to stablish the role of the C-particles in the present model: i) If w_{BC}=0.0, the particles only block the adsorption sites and decrease de coordination of adsorption sites. ii) If $w_{BA} \neq w_{BC}$ the C-particles are of different nature from the seed (A- particles); this is the case, for example, of a site blocking monolayer of organic or inorganic species on the surface. If C particle are metals, distortions can significantly affect the coordination of the NP atoms and, therefore, the energetics of the

system [62], iii) Finally if $w_{BA} = w_{BC}$, the C-particles can be considered as surface defects of the same kind of the seed, in this case surface distortions can be neglected.

In the present work only the case iii) is considered, so *C–particles will be of the same nature as the seed*. In the following, for simplicity, we will refer to these particles as "defect particles" and it will be only necessary to define the value of w_{BA} to also define w_{BC}, since always $w_{BA} = w_{BC}$. If there are N_d defect particles on the surface it is possible to define the *surface defects density* by $\sigma = N_d/N$, being $0.0 \leq \sigma \leq 1.0$. Here σ is a measure of the quantity of structural defects present on the NP surface, normalized by the total surface sites. When $\sigma=0$, the NP has no surface defect, is clean. So, given an σ value, the quantity of available adsorption sites is $M=N-N_d$.

With these considerations the equation (1) take the form:

$$H(N,\sigma) = \frac{1}{2}\sum_{<i,j>}\left(w_{BB}\,\delta_{c_i,-1}\delta_{c_j,-1} + w_{BA}\,\delta_{c_i,-1}\delta_{c_j,1}\right) - \mu\sum_{i}^{M} c_i \qquad (2)$$

In the present model the multi-layer is prohibited. The adsorption-desorption equilibrium process is simulated by Monte Carlo technique in the Grand Canonical Ensemble, using the Glauber algorithm [26, 63]. The Metropolis scheme [64] is used to satisfy the principle of detailed balance. The equilibration method of Monte Carlo simulation, consists on trying to change the occupation status of the adsorption sites, randomly chosen, with the aim of minimizing the global energy of the system. If the site is empty the method will try to fill it and vice versa. A Monte Carlo step (MCS) is achieved when each of the M-N_d sites has been tested to change. Typically, the equilibrium state can be well reproduced after discarding the first 5×10^6 MCSs. Then, the next 2×10^6 MCSs are used to compute averages. 1000 different initially random configurations were used. The typical thermodynamics parameters are measured as usual. The mean coverage is obtained as:

View Article Online
DOI: 10.1039/D0CP03348K

$$\theta(\mu) = \frac{\left\langle \sum c_i \right\rangle}{M} \quad , \qquad (2)$$

If θ=0.0, the surface is empty of B-particles, but if θ=1.0 all available sites are occupied. Energy per site;

$$E_s = \frac{\langle H(M, N_d) \rangle}{M} \qquad (3)$$

Compressibility of the adlayer;

$$k_B T \left(\frac{\partial \theta}{\partial \mu} \right) = \left\langle N_B^2 \right\rangle - \left\langle N_B \right\rangle^2 \qquad (4)$$

This quantity is proportional to the current measured in a voltammetric experiment [65]. The derivative $\partial\theta / \partial\mu$ can be computed in the Grand Canonical ensemble via the normalized mean square fluctuations from the thermodynamics fluctuation theory [66, 67]. The brackets mean the average over the MC simulation runs.

3 Results and discussions

3.1. Structural surface analysis

First, we will analyze the surface structure with statistical calculation for the clean NP($\sigma = 0$) and with defects ($\sigma \neq 0$). For this analysis, the surface is considered free of B-particles. In a NP different environments can be identified around an empty site, depending on the number of links with both defect particles or atoms from the seed. So, an environment is defined in the present work as the number of links of an empty site with the atoms that surround it.

To understand the surface structure and the energetic associated with the environments, we will compute the *adsorption sites distribution* f_n. Being "*n*" the number of links

View Article Online
DOI: 10.1039/D0CP03348K

which defines a particular environment, as we have already mention. In other words, f_1 is number of empty sites with a single link divided by M, f_2 is number of empty sites with two links divided by M and so on. f_n depend on σ and NP geometry, then $\sum_n f_n = 1.0$.

In a clean ICO NP (σ = 0.0), there are three types of superficial sites, where an external particle can be deposited: vertices sites (n=1), borders sites (n=2), and facets sites(n=3). For this geometry it is possible to obtain the distribution throughout equations:

$$f_1(\sigma = 0.0) = \left.\frac{6}{5\alpha^2 + 1}\right|_{\alpha=8} = 0.018, \qquad f_2(\sigma = 0.0) = \left.\frac{15(\alpha - 1)}{5\alpha^2 + 1}\right|_{\alpha=8} = 0.32 \qquad \text{and}$$

$$f_3(\sigma = 0.0) = \left.\frac{5(\alpha^2 - 3\alpha + 2)}{5\alpha^2 + 1}\right|_{\alpha=8} = 0.65.$$ Where α is a natural number, which denotes the "α-esimo" member of the geometrical family to which the ICO NP belongs. The smallest icosahedra is identified by α=1, and is formed by 13 atoms , α=2 correspond to a ICO NP with 55 atoms and so on. In our case α = 7 correspond to 1415 atoms from the core and there are 642 sites from the shell. Note that in the previous equations we consider α = 8, since it corresponded to the complete NP (core + shell). So the kind of site that mostly contributes to energy are the facets, since $f_3(\sigma = 0.0) = 0.65$. These expressions were reported in the reference [44].

However, in an ICO NP with surface defects (σ≠0.0) the distribution of environments varies with σ , as we will show briefly, with n ranging from 1 (adsorption site placed on a vertices site, without defects surrounding it) to 9 (adsorption site placed on a facet site, surrounded by 6 defects). Some of these environments are illustrated in figure 1 for an ICO NP with N_A=1415 and σ=0.1. The seed A-atoms are identified with dark green circle and the defect particles with yellow circles. White circles are used to identify a few adsorption empty sites and the number inside those circles indicates the amount of links which characterize the environment. The insert shows a zoom of the

selected environments, to provide a detailed picture of them. As observed in figure 1, those environments with n=1, 2, 3 has only links with 1, 2 and 3 atoms from the seed, respectively. However, for n=4, the empty site has 2 links with the seed and other 2 links with the surface defects. For n=5, there are 3 links with the seed and 2 with the surface defects. These examples are arbitrary and only show one of the possible configurations for the considered environments. Note that, for example, the environment n = 3 can be constructed in 3 different ways: i) one link with the seed and two with the defects, ii) two links with the seed and one with the defects and iii) three links with the seed without defect links. The case iii) is the only one present in the clean ICO NP. This gives an idea of the complexity of the case where σ≠0.0 compared to that where no defects are involved, and the need to use statistical measures to aboard the present phenomenon.

Figure 1

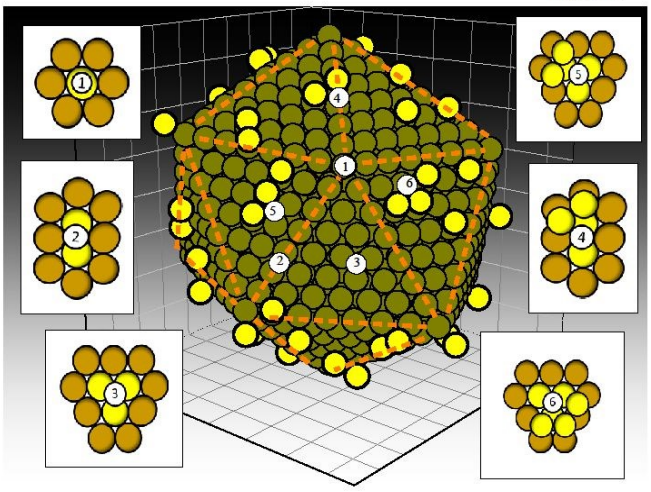

Figure 1: Snapshot of ICO NP of N_A=1415 with σ=0.1. The seed atoms are identified by green circle, the defect particles in yellow circles. White circles indicate a few adsorption sites. The insert shows a zoom of each environment.

As we have said previously, when σ≠0.0 the computing is not so simple, since the system is highly degenerated because defect particles are randomly deposited on the

surface sites. So, it becomes necessary to compute statistics samples. With an appropriate number of random samples, it is possible to obtain the average distribution, with a negligible statistical error (less than 2%).

Three adsorption site distribution for σ=0.0, 0.5 and 0.9, are shown in figure 2. f_n was measured and averaged from 100000 random configurations of a ICO NP with N_A=1415. As expected, σ=0.0 has 3 environments, n=1,2,3, with frequencies $f_1(\sigma = 0.0)$, $f_2(\sigma = 0.0)$ and $f_3(\sigma = 0.0)$, as previously commented. For σ = 0.5, the most frequent environment is n=6, this means that this is the most likely environment to find in a statistical sample. Then, figure 2 shows that, for σ=0.9, n=8 is the most important environment. For the former case, the distribution maxima shifts toward larger environments compared to σ = 0.5, in fact those with n≤3 have completely disappeared.

Figure 2

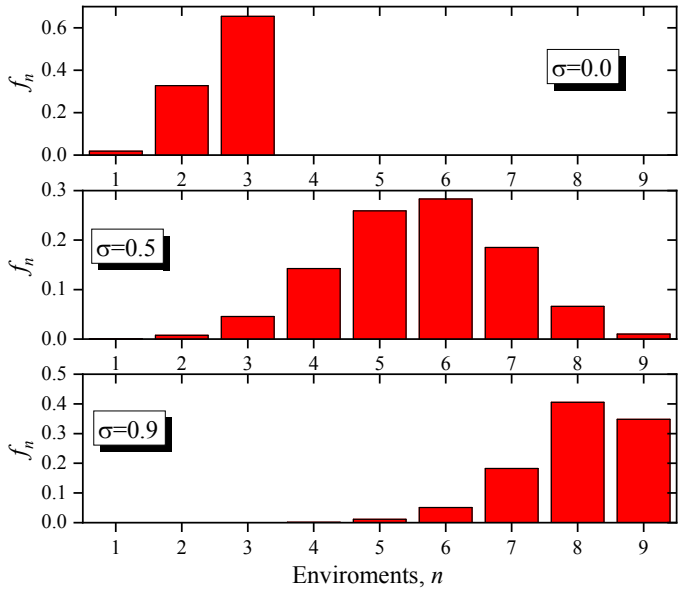

Figure 2: The adsorption site distribution f_n for the ICO NP(N_A=1415) for σ values indicated.

The distribution f_n is expected to depend on the NP size and σ. The clean ICO NP behavior in the limit where $N_A \to \infty$ is well known. There are algebraic expressions that quantify the amount of sites, N_{edges}, $N_{vertices}$, and N_{facet} for different sizes [44]. As N_A increase, the ICO NP tend to a two dimensional surface. In other words, when $N_A \to \infty$, the surface density of edge sites (N_{edges}/N) and vertices sites ($N_{vertices}/N$) tend zero, however the density of facet sites (N_{facet}/N), tend to 1, this correspond to a triangular lattice surface. In figure 3(a) those theoretical expressions, $f_n(\sigma=0.0)$, for n=1,2 and 3 are plotted versus N_A, for a clean nanoparticle. The number on the lines indicates the "n" value. The environments 1, 2 and 3 correspond to vertices, border and facet sites respectively. Clearly, as N_A increase , the environment 3 increase and the others decrease. This is correct because in the limit $N_A \to \infty$, the NP tend toward a triangular surface where n=3 is the most likely environment and n=1 and 2 becomes negligible.

The other distributions, where $\sigma \neq 0.0$, are showed in figure 3(b), (c) and (d) for different sizes and σ for different values. These results were obtained by computing statistic samples, since there are no simple algebraic expressions to describe the distribution features, as the clean case. As expected, from the link distribution analysis, more environments are observed compared to the σ=0.0 case.

View Article Online
DOI: 10.1039/D0CP03348K

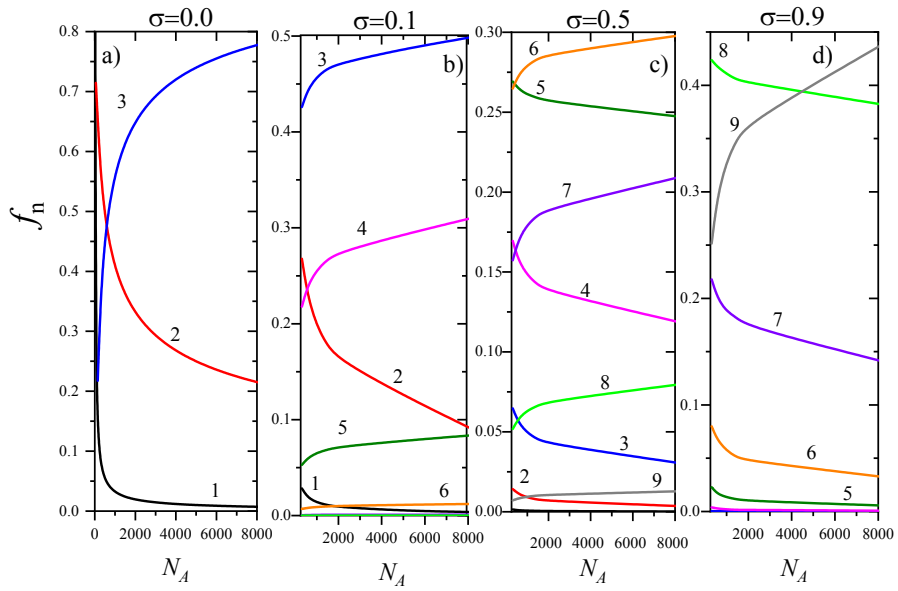

Figure 3

Figure 3: Adsorption sites distribution vs NP size for different cases: a) σ=0.0, b) σ=0.1, c), σ=0.5 and d) σ=0.9. The different curves correspond to different environments, the number above them label the environment considered. To guide the eye, the same environments are represented in a), b), c) and d) with the same colors.

For σ=0.1 , see Figure 3(b), f_n rises with N_A for n=3,4,5 and 6, and decrease for n=1 and 2. This behavior is understandable because the environments n=1, 2 can only be placed on edges and vertices sites, whose tendencies are to decrease with size, as already seen, and the rest of the environment with $n>2$ are most likely formed on facets, which increase with size. Figure 3(c) , show the case associated with σ=0.5. In this case, the half of the total sites are occupied by defect particles. So, in average, the half of neighbors of each of the available adsorption sites are occupied by defect particles. Thus, in average, the environments with $n\leq 5$ can be associated with vertices and edges sites, and tend to decrease with size. The environments 1 and 2 are the less probably and tend to disappear at larger values of N_A. The rest of environments with $n>5$ are formed on facets sites, as N_A increase, and are expected to increase with size, as observed. Finally, distribution for σ=0.9 is showed in figure 3(d). At this σ value only the highest environment n=9 increase,

since 10 % of the total sites are available and n=9 can exclusively be formed on facets. As the amounts of these sites increase with N_A, then the distribution of n=9 increases too. The rest of the environments with $\underline{n}$<9 are most probably to find on borders, so distribution is expected to decrease with size.

3.2 Monte Carlo results and discussions

To analyze the thermodynamics features that arise with the present model, MC method, described in section 2, is applied to the same ICO NP with N_A=1415 used for the surface analysis in the previous section. In this instance, pairwise interactions may seem insufficient to study metallic nanosystems, however the main characteristics of the surface decoration of metallic NPs, carried out with more refined models such as the Embedded Atom Method (EAM) [68], show characteristics very similar to those observed with the Hamiltonian presented in this work. The model with pairwise interactions is useful for a first study, where the general characteristics of the system are understood and serving as a starting point for more specific studies. As we said, this work does not seek to describe any specific system, but rather to identify the most relevant characteristics. The results of this model serve as a fundamental basis to deepen a study of specific systems. We are currently developing a study of the decoration of NP with impurities with EAM, we seek to understand the behavior of metallic systems with a more realistic vision. In supplementary information we compare and discuss two isotherms(see fig S1) for a clean ICO NP, obtained with EAM and pairwise interactions.

Following this work we consider lateral attractive interactions being w_{BA}/k_BT = -15.0 and w_{BB}/k_BT = 0 with k_BT=1.0. Here k_B is the Boltzmann constant and T the temperature. The condition w_{BB}/k_BT = 0.0, considers that there are no interactions between two atoms of species B and is equivalent to $w_{AB} >> w_{BB}$. The purpose of this condition is to explicitly expose the effect of the surface structure by canceling the energetic emerging

from the interaction between adsorbates. In the case that $w_{BB}/k_BT \neq 0.0$ would be considered, this would lead us to a more complex scenario, since the NP-adsorbate energetics would be superimposed with the adsorbate-adsorbate energy. These types of interactions are commonly used in metal simulations. For each case, a potential window in order to observe the complete adsorption process is used.

Mean coverage versus chemical potential (isotherms), for several values of σ are shown in figure 4 (a). Some important observation can be made. In the clean NP (σ=0.0), the surface coverage θ increases from zero to one. In total, four plateaus are formed, at θ=0.0, 0.65, 0.97 and 1.0. The first and last values indicate empty and full surface coverage, respectively. The second plateau correspond to the filling of the facet sites only, where each B-particle is linked with three NNs of the seed. The third plateau corresponds to the filling of facet plus the edge sites. This phenomenology was reported in reference [44] for clean ICO NPs. For the rest of the isotherms where σ≠0.0, it can be see how they all move towards lower chemical potentials as σ increases, and five "extra" plateaus appear. At the moment, the nature of these other plateaus is unknown, but we will back to this point later.

Now let us analyze the compressibility of the adlayer, or the derivative of the isotherm previously detailed in equation (4). This expression is related to the calculus of the current in electrosorption voltammograms simulations [29]. Figure 4 shows compressibility of the adlayer, and isotherms versus chemical potential for several σ values. The compressibility peak maximums correspond to the inflexion points observed in the isotherm, this fact is pointed with dashed lines connecting the inflection points in Figure 4 (a), with the maximums in Figure 4(b). By other side, the minimums in the compressibility are related to occupation plateaus founded in the isotherms; for example, for σ=0.0 (black line), the four minimums are related to the four plateaus observed in the

isotherms (black symbol). Another useful observation can make: for a pair of consecutive plateaus of Figure 4 (a), called arbitrary i and j, the difference on the surface coverage $\Delta\theta = \left|\theta_j - \theta_i\right|$, is proportional to the height of the peak arising from the jump *i-j* in Figure 4 (b). For example, the major peak in Figure 4(b) for σ=0.0 is observed when the biggest coverage jump ($\Delta\theta$) occurs. In the same way, the second peak height corresponds to the second $\Delta\theta$, and so on. The importance of the compressibility peaks behavior to analyze surfaces in detail has been demonstrated in a previous work [29], but in the present case, the thermodynamic data presented is insufficient to understand by itself the nature of the peaks.

Figure 4

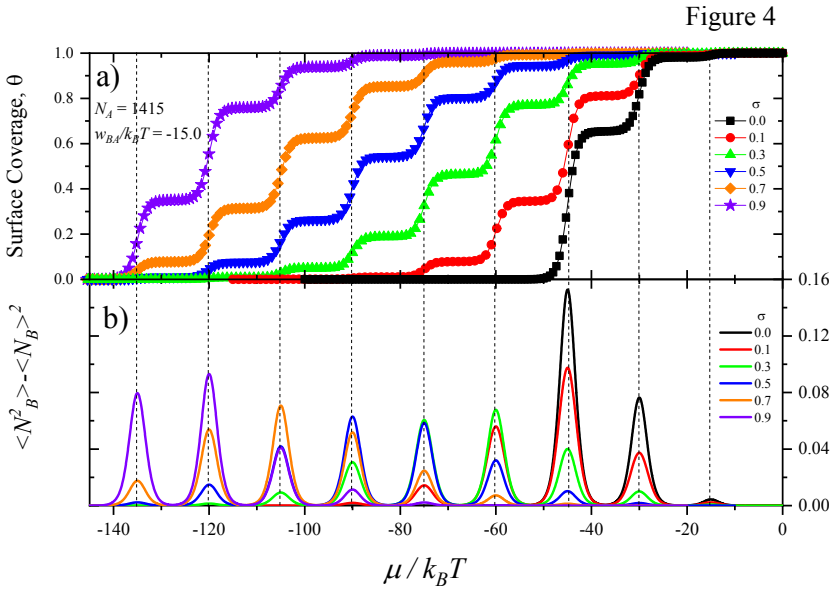

Figure 4 : a) Isotherms, b) Compressibility of the adlayer, versus chemical potential, for the σ values indicated . Dashed lines were added to guide the eye.

With the structural surface analysis of section 3.1, it is possible to interpret the phenomenon observed in MC simulations. Figure 5 shows the isotherm and energy per

View Article Online
DOI: 10.1039/D0CP03348K

site versus chemical potential for σ=0.1, the same analysis can be tackled with the rest of σ values. As expected, each plateau of the isotherm (in red) can be associated with a plateau from the energy per site (in blue). For a better analysis, plateaus are labeled from A to G, and the numbers indicate different inflexion points. At low coverage, the inflection point 6 connects plateaus A and B. From the distribution in the inset (i), it can be observed that there are 6 possible environments with n=1,2,3,4,5, and 6. Thus, the jump 6 from A to B can be related to the filling of the environments *n*=6, since this environment corresponds to the lower local energy, because the empty site is surrounded by 6 attractive neighbors. In the same way, the rest of the plateaus B, C, D, E, F and G are formed by the consecutive filling of environments *n*=5,4,3,2 and 1 as the chemical potential increase (becomes more positive), respectively. Because, following the same *n* order, the attractive local energy decreases. But, statistical calculations from section 3.1 predicts very small distributions for *n*=7 (f_7 = 0.00079) and *n*=8 (f_8 = 0.00002), these values cannot be observed in the inset i) with a clean eye. Looking in detail, a plateau in the energy per site and other in the isotherm are observed previous to the plateau A in the insets (ii) and (iii), respectively. In the inset iii), it can be seen the small jump 7 to form the plateau A, with an occupation smaller than 0.001, this jump can be related with the filling of *n*=7 environments. This results strongly suggest that the plateau A must be composed of *n*=8, 7 environments, the plateau B of *n*=8,7,6, C of *n*=8,7,6 and 5, and so on, until the last plateau which must contain all the possible environments.

View Article Online
DOI: 10.1039/D0CP03348K

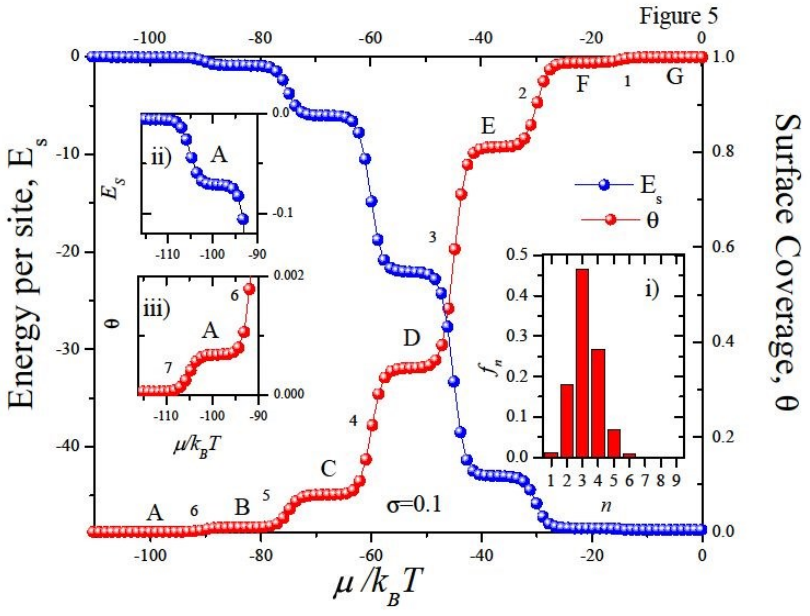

Figure 5 : Isotherm and energy per site versus chemical potential in unit of k_BT , for σ=0.1 and w_{BA}/k_BT = -15.0 . Inset i) adsorption site distribution .The insets ii) and iii) shows a "zoom" of plateaus, of the isotherms and energy per site respectively.

If these plateaus compositions hypothesis are correct, the energy per site calculated with MC simulations for each of the plateaus, must coincide with the energy calculated with the adsorption site distribution f_n, with the same energy values from MC simulations. Is possible to obtain the energy per each environment with the adsorption sites ditribution as $e_n = nf_n w_{BA}$ and the total energy per site $E_s = \sum_n e_n$. The results of the energy per site calculated with f_n and the composition details supposed for each of the plateau of Figure 5 are showed in Table 1. It can be seen that the energy per site predicted for the plateau A ($E_s^B = e_7 + e_8 \approx -0.07$) is equal to that showed in the inset ii) of Figure 5. In the same way, the energy per site predicted for the plateau B ($E_s^B = e_6 + e_7 + e_8 \approx -0.9$) is the same as that showed in the energy plateau B. Taking the plateau D (n=8,7,6,5,4) as another example, the energy from Table 1 predicts a value of

$E_s^B = e_4 + e_5 + e_6 + e_7 + e_8 \approx -22.0$, which is exactly the same observed for D in figure 5. The same coincidences are observed for plateaus E, F and G. Hence, we can safely say that plateaus and compressibility peaks are associated to the filling of the different environments generated over the nanoparticle surface by the parameter σ.

It is possible to easily extent this analysis to other schemes with other σ values as those from Figure 4, but we believe that the previously developed analysis is clear enough to move on.

Plateau	**E_s**	**Environments**	**Surface Coverage**
A	-0.07	7,8	6.8×10^{-4}
B	-0.9	6,7,8	0.009
C	-6.0	5,6,7,8	0.07
D	-22.0	4,5,6,7,8	0.345
E	-43.0	3,4,5,6,7,8	0.81
F	-48.3	2,3,4,5,6,7,8	0.98
G	-48.51	1,2,3,4,5,6,7,8	1.0

Table 1 : Plateau, energy per site , environments and surface coverage for data show in figure 5.

Now we are interested in understood the phenomenology when the relation w_{BA}/k_BT changes. When temperature increases or the interaction energy decrease, the thermal fluctuation begins to play an important role in the deposition process. Figure 6

shows compressibility of the adlayer versus chemical potential for several w_{BA}/k_BT values and constant σ=0.1. The inset shows the corresponding isotherm for each of the cases. At $w_{BA}/k_BT = 0.0$, the compressibility shows a single peak, in concordance with the sigmoid curve observed in the isotherm. In this situation, the compressibility and the isotherm behavior are well understood since the process is controlled by thermal fluctuations and deposition occurs randomly (Langmuir conditions). However, when w_{BA}/k_BT decreases from 0 to -30, several peaks are gradually formed in correspondence with the plateaus observed in the isotherms, because lateral interactions govern the process. Peaks intensity and the separation between them, depends on the energy values.

Figure 6

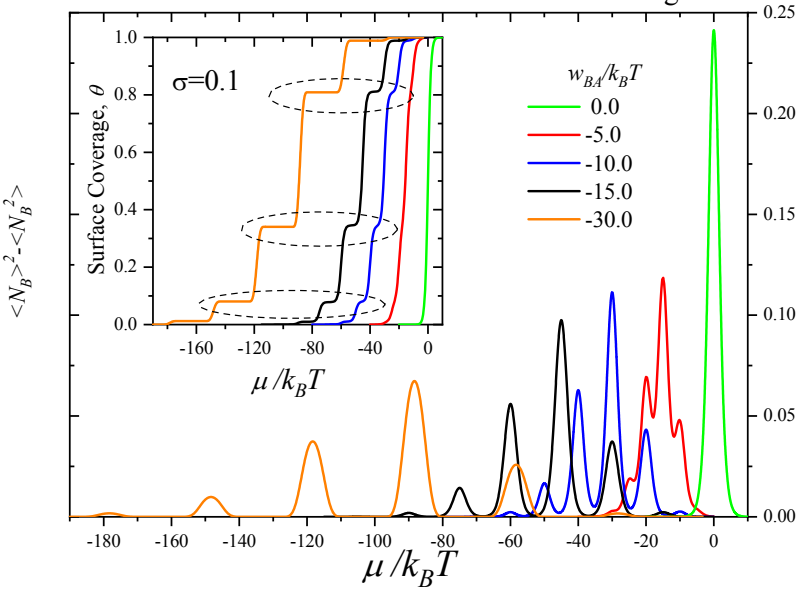

Figure 6: Compressibility of the adlayer versus chemical potential at σ=0.1 fixed, for several values of w_{BA}/k_BT, inset shows the correspondent isotherms

If $|w_{BA}/k_BT|$ increase, less chemical potential must be exerted to insert a particle on the NP surface. This is manifested as an increase in the size of the plateaus (as is indicate by ellipse in the inset of figure 6) and a shift towards negative potentials of the observed peaks.

View Article Online
DOI: 10.1039/D0CP03348K

To clarify this phenomenon figure 7 shows the behavior of the compressibility for different σ and different w_{BA}/k_BT values. The panel a) shows the case for w_{BA}/k_BT =-3.0 where the peaks for each σ tend to overlap , because is close to the regimen of high temperature (Langmuir case, w_{BA}/k_BT =0.0), where thermal fluctuations dominate, and thus the deposition occurs randomly, as we have already discussed. On the other hand, when the interactions become more negative, the thermal fluctuation is less invasive, and the plateaus become more defined, the panel b) to d) show this behavior. One important conclusion can be drawn looking at all figures from a) to d): the position of the peaks on the chemical potential axis only depends on w_{BA}/k_BT , but not on σ. The peaks separations are greater as the interactions are more attractive.

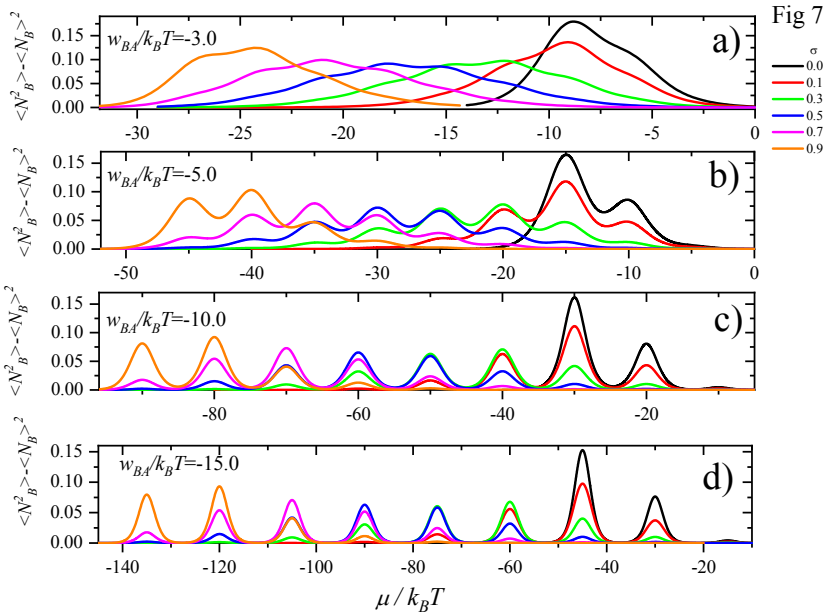

Figure 7 : Compressibility versus chemical potential at different values of energy and σ indicated .

As is known for nanosystems, the size and geometry play an important role on surface processes. In particular, we are interested in analyzing the thermodynamic

dependence of NP size for w_{BA}/k_BT =-15.0 and σ=0.1. For a better visualization of the effect that the nanoparticle size has on the process, we show the data without normalizing by the number of available sites and the isotherm as N_B (total number of B-particles) versus μ/k_BT. The panel a) in figure 8 shows isotherms for several NP sizes N_A. For all the sizes, the width of the plateaus is not altered, and the inflexion points do not suffer displacements in the chemical potential axis. These observations are in correspondence with what was observed in the compressibility peaks, shown in figure 8 b). That is to say, all peaks maximums are observed in the same chemical potential values and the peak intensity increases with N_A The inset shows a zoom for the peak at μ/k_BT<-100.

Fig 8

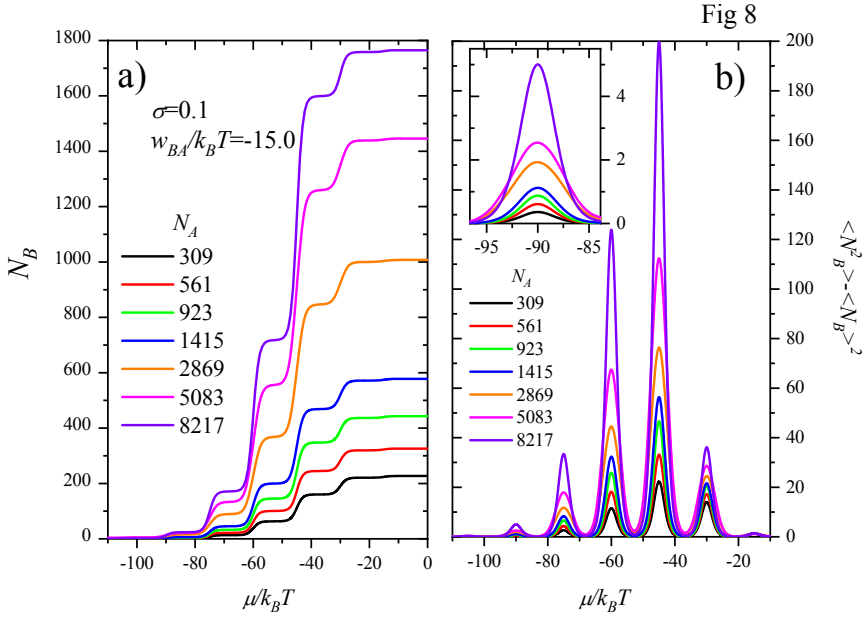

Figure 8 : a) Isotherms (not normalized) for several values of N_A . In this case the isotherms are presented by N_B(number total of B-particles) versus μ/k_BT. b) Compressibility respective.

In experimental studies, frequently the substrates are formed by several kinds of NPs, with different geometries. Even in this complex scenario, valuable information is possible to obtain analyzing the behavior of a clean NPs. A clean cuboctahedral (CO) and truncated octahedron (TO) NP are formed by two different kind of facets, sites with

five NNs (square geometry) and nine NNs (triangular geometry). These nanoparticles are showed in figure 9 (a) and (b). Figure 9 (c) shows the compressibility of monolayer for ICO , CO and TO NPs for σ=0.1, with similar size and interaction energies as indicated in the figure. Green line point the convolution for the different NP responses. This islike the "experimental noise" observed in experimental voltammograms, generated by different geometries with similar sizes. For all NPs, the peaks coincide in the chemical potential position and the number above the peaks indicate the environment associated with the filling of the sites at that point. This reveals that the same environments from different substrates are identified at exactly the same chemical potential position. This is an evidence that the peak position depends on *n* and so on the local energy of the environment, but not on the geometry. The inset show a zoom of the environment n=7.

Fig. 9

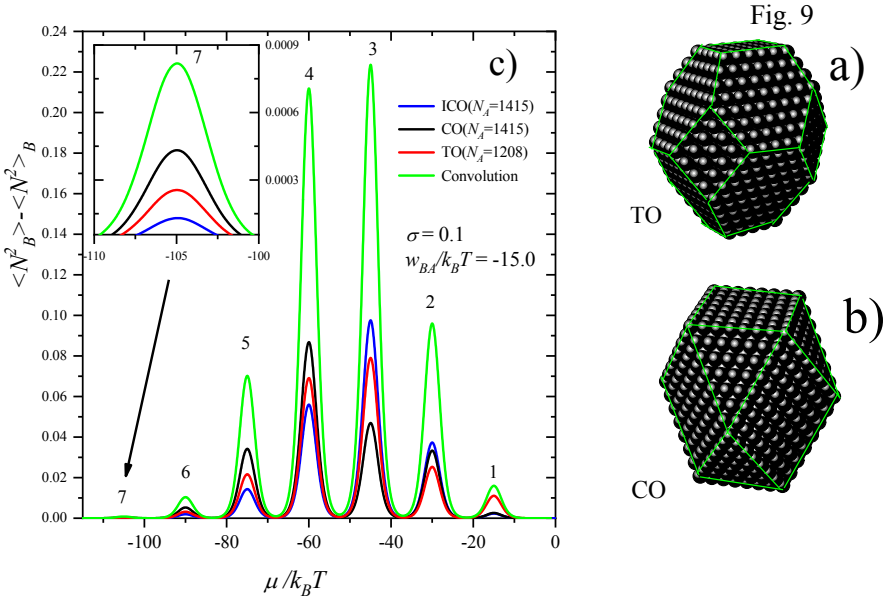

Figure 9: a) Truncated octahedron (TO) NP. b) Cuboctahedral(CO) NP. c) compressibility for ICO , CO and TO NPs with similar size and energies as is indicated. Green line indicates the convolution of all them. The inset show a zoom of the environment n=7.

3.0 Conclusions

View Article Online
DOI: 10.1039/D0CP03348K

In the present study, a detailed characterization of surfaces with defects of various types of nanoparticle geometries has been achieved, using Monte Carlo simulations and statistical calculations. The methodology was applied in order to develop a simple method for the structural analysis of the surface that could serve as a tool, or a reference, for the interpretation of the results with more complex and specific models. It was possible to interpret relevant details of the complex surface of a nanoparticle with defects using statistical measurements. This lead us observe different adsorption sites distributions, related to the coordination number or "environments" as we have denominated during the work, which depends on the geometry, the degree of surface defects and the size of the nanoparticle. Then, it was possible to link the statistical results with Monte Carlo simulations to describe how the degree of surface defects influence the behavior of the compressibility of the adlayer and other thermodynamic parameters. The results strongly suggest that the energetics emerging from the defective surface, rules the thermodynamics at low temperature conditions or strong attractive interactions, where the structural details are clearly manifested. Finally, we adapted the model to laboratory conditions, to predict the behavior of these systems as in hypothetical real experiments. In such conditions, the details of the surface heterogeneity vanish as temperature becomes more important.

In particular, several observations can be highlighted:

i) The surface defects density, measured by σ, induce the formation of different environments with "*n*" links. These environments define a site distribution for the adsorption phenomena and are manifested in the isotherms as broad plateaus and peaks in the compressibility of the adlayer.

ii) The distributions f_n of the environments depend on NP size and surface defects density.

View Article Online
DOI: 10.1039/D0CP03348K

iii) These environments only can be observed at low temperatures. When temperature increases the environments cannot be clearly identified.

iv) For a unique NP geometry, the intensity of compressibility peaks, depend on N_A nanoparticle seed, but do not show displacement in chemical potential.

v) For constant σ, and different nanoparticle geometry, all the environments are identified at the same values of chemical potential, but with different voltammogram peaks height, since each geometry has a different link distribution.

vi) The compressibility of the adlayer peaks position shifts of chemical potential with temperature changes.

This is a first, necessary, step to link a complete surface structure analysis with the response observed in electrochemical and thermodynamic measurements. Our goal is that the results and discussions from the present work can help to understand the results of simulations with complex and specific models.

Conflicts of interest

There are no conflicts of interest to declare

6. Acknowledgements

This work was supported in part by CONICET (Argentina) under project number PIO 112-201101-00615. Universidad Nacional de Santiago del Estero(Argentina), under project CICyT-UNSE 23 /A241. The simulations were carried out on a HUAUKE parallel cluster located at Instituto de Bionanotecnología del NOA, Universidad Nacional de Santiago del Estero, Santiago del Estero, Argentina.

References

[1] M. Ishigami, H. J. Choi, S. Aloni, S. G. Louie, M. L. Cohen, and A. Zettl, Phys. Rev. Lett. 2004, **93**, 196803.

[2] S. V. Kuchibhatla, A. S.Karakoti, D. Bera, and S. Seal, 2007, Prog. Mater. Sci. , 2007, **52**, 699.

[3] S. George, S. Lin, Z. Ji, C. R Thomas, L. Li, M. Mecklenburg, , ... and J.N .Hohman, ACS nano, 2012, **6**, 3745.

[4]A. Naldoni, M. Allieta, S. Santangelo, M. Marelli, F. Fabbri, S. Cappelli, ... and V. Dal Santo, J. Am. Chem. Soc., 2012, **134**, 7600.

[5] B. I . Yakobson and P. Avouris, *Mechanical properties of carbon nanotubes. In Carbon nanotubes* , Springer, Berlin, Heidelberg, 2001.

[6] D. L Fedlheim , and C. A. Foss, *Metal nanoparticles: synthesis, characterization, and applications*. CRC press, 2001.

[7] C.N.R. Rao, A. Müller and A.K.Cheetham, *The Chemistry of Nanomaterials: Synthesis, Properties and Applications* (2 vols.). Wiley-VCH, Weinheim, Germany, 2004.

[8] C. Altavilla and E. Ciliberto, *Inorganic Nanoparticles: Synthesis, Applications and Perspectives,* CRC Press, 2017.

[9] L. Piot, S. Le Floch, T. Cornier, S. Daniele, and D. Machon, (2013). J. Phys. Chem C, 2013, **117**, 11133.

[10] C. Xie, J. Hu, R. Wu, and H. Xia, Nanostruct. Mater. , 1999, **11**, 1061.

[11]M. Quintana, E. Haro-Poniatowski, J. Morales, N. Batina, Appl. Surf. Sci. 2002, **195**, 175.

[12] T. Donnelly, S. Krishnamurthy, K. Carney, N. McEvoy and J.G., Lunney, Surf. Sci. 2007, **254**, 1303.

[13] Z. Wu, W. Li, M. Zhang, and K. Tao, Front. Chem. Eng. China, 2007, **1**, 87.

[14] L. Machala, R. Zboril, and A. Gedanken, J. Phys. Chem. B, 2007, **111**, 4003.

[15]R.S. Dhumal, S.V. Biradar, S. Yamamura, A. R. Paradkar and P. York, Eur. J. Pharm. Biopharm. 2008, **70**, 109.

[16] Z. Bartul and J. Trenor, *Advances in Nanotechnology*, Vol. 4. Nova Science, New York, USA, 2010.

[17]K.S. Sattler, Handbook of Nanophysics: Nanoparticles and Quantum Dots. CRC Press, New York, 2016.

[18] V. Van Hoang, and D. Ganguli, Phys. Rep. 2012, **518**, 81.

[19] J.M. Ilnytskyi, A. Slyusarchuk and M. Saphiannikova, Macromolecules, 2016, **49**, 9272.

[20] F. Carnal, and S. Stoll, J. Phys. Chem. B, 2016, **120**, 7988.

[21] D. Toghraie, M, Mokhtari and M Afrand, Phys. E, 2016, **84**, 152.

[22] M.K. Alam, S. Saito, and H. Takaba, J. Mater. Res., 2017, **32**, 1573.

[23] T. Nann and J. Heinze, Electrochem. commun., 1999, 1, 289.

[24] R. G. Compton, E. Laborda, and K. R. Ward, *Understanding Voltammetry: Simulation of Electrode Processes,* Singapore, 2013.

[25] D. Britz, *Digital Simulation in Electrochemistry*, Third. Berlin, Heidelberg, 2005.

[26] K. Binder, Simulation of Diffusion in Lattice Gases and Related Kinetic Phenomena, Applications of the Monte Carlo Method in Statistical Physics, Topics in Current Physics V, Springer, Berlin, 1987.

[27] A. J. Bard, J. A. Crayston, G. P. Kittlesen, T. Varco, and M. S. Wrighton, Anal. Chem. 1986, **58**, 2321.

[28] H. Yang and A. J. Bard, J. Electroanal. Chem. Interfacial Electrochem, 1991, **306**, 87.

[29] E.G. Arriazu and O.A Pinto. App. Surf. Sci. 2018, **433**, 705.

[30] E.A. Rikvold, M. Gamboa-Aldeco, J. Zhang , M. Han , Q. Wang , H.L. Richards and A. Wieckowskic, Surf. Sci.1995, **335**, 389.

[31] J. Zhang, Y. Sung , P. A. Rikvold and A. Wieckowski, J. Phys. Chem, 1996, **104**, 5699.

[32] S. J. Mitchell, G. Brown and P. A. Rikvold, J. Electroanal. Chem, 2000, **493**, 68.

[33] I. Abou Hamad, T. Wandlowskic, G. Brown and P. A. Rikvold, J. Electroanal. Chem 2003, **554**, 211.

[34] K. Binder, *Monte Carlo Methods in Statistical Physics (Topics in Current Physics)*, Springer, Berlin, 1978.

[35] K. Binder, Rep. Prog. Phys. 1997, 487.

[36] K. Binder and D. Heermann, *Monte Carlo Simulation in Statistical Physics - An Introduction*, 5th ed. Springer, Berlin, 2010.

[37] P. M.Pasinetti, J. L. Riccardo, and A.J. Ramirez-Pastor, Physica A: Statistical Mechanics and its Applications, 2005, **355**, 383.

[38] O.A. Pinto, P. M. Pasinetti, F. Nieto, and A. J. Ramirez-Pastor, J. Phys. Chem, 2011, **134**, 064702

[39] N.B. Luque, M. G. Del Pópolo and E. P. M.Leiva, Surf. Sci., 2004, **571**, L319.

[40]O.A. Pinto, B. L. de Mishima, E. P. M. Leiva and O. A Oviedo, Phys. Chem. Chem. Phys., 2017, **19**, 1601.

[41] A. Clavier, F. Carnal, and Stoll,. J. Phys. Chem B, 2016, **120**, 7988.

[42] O. A. Pinto, B. L. de Mishima, E.P.M. Leiva, O.A. and Oviedo. Phys. Chem. Chem. Phys, 2016, **18**, 14610.

[43] O. Iglesias and A. Labarta, A. Phys. Rev. B, 2001, **63**, 184416.

[44] O. A. Pinto, B. L. de Mishima, M. Dávila, A. J. Ramirez-Pastor, E. P. M. Leiva, , and O. A. Oviedo, Phys. Rev. E, 2013, **88**, 062407.

View Article Online
DOI: 10.1039/D0CP03348K

[45]S. Monti, V. Carravetta, and H. Ågren, Nanoscale, 2016, **8**, 12929.

[46] V.V. Hoang and T. Odagaki, Phys. Rev. B 2008, **77**, 125434 .

[47] V.V. Hoang, N. H. T. Anh and H. Zung, Physica status solidi (b) 2008, **245.8**, 1505.

[48]Y. Shibuta, and T. Suzuki, Chem. Phys. Lett. , 2007, **445**, 265.

[49] Q. Zeng, X. Jiang, A. Yu, and G.M. Lu, Nanotechnology, 2007, **18**, 035708.

[50] P. H. Kien, M. T Lan, N. T. Dung, and P. K. Hung, Int. J. Mod. Phys. B , 2014, **28**, 1450155.

[51] K. Yun, Y. H. Cho, P. R. Cha, J. Lee, H. S. Nam, J. S. Oh, , ... and S.C. Lee, Acta Mater. ,2012, **60**, 4908.

[52] L. Tun-Dong, Z. Ji-Wen, S. Gui-Fang, F. Tian-E, and W. Yu-Hua, Chin. Phys. B, 2015, **24**, 033601.

[53] O. A. Pinto, B. A. Lopez de Mishima, E. P. M. Leiva and O. A. Oviedo, Phys. Rev. E 2012, **86**, 061602.

[54] K. H. Kuo, Struct. Chem., 2002, **13**, 221.

[55] D. Bochicchio and R. Ferrando, Nano lett. 2010, 10, 4211.

[56] A. L. Mackay, Acta Crystallogr. 1962, **15**, 916.

[57] H. Y. Kim, J. O. Sofo, D. Velegol, M. W. Cole and A. A. Lucas, J. Phys. Chem, 2006, **124**, 074504

[58] C. A. S. Batista, R. G. Larson and N. A.Kotov, Science, 2015, **350**, 1242477.

[59] M. M. Mariscal, O. A. Oviedo and E. P. M. Leiva, J. Mater. Res 2012, **27**, 1777.

[60] B. Shan, L. Wang, S. Yang, J. Hyun, N. Kapur, Y. Zhao, , ...and K. Cho, Phys. Rev.

View Article Online
DOI: 10.1039/D0CP03348K

B, 2009, **80**, 035404.

[61] H. Y. Kim, J. O.Sofo, D. Velegol, M.W. Cole and A.A. Lucas, J. Phys. Chem, 2006, **124**, 07450.

[62] D. Nelli and R. Ferrando. Nanoscale, 2019, **11**, 13040.

[63] K. Binder , Applications of the Monte Carlo, Method in Statistical Physics, Vol. Springer, Berlin, 1984.

[64] N. Metropolis, A. W. Rosenbluth, M. N. Rosenbluth, A. H. Teller, and E. Teller, J. Chem. Phys., 1953, **21**, 1087.

[65] G. Brown, P. A. Rikvold, S. J. Mitchell and M. A. Novotny, Monte Carlo methods for Equilibrium and Nonequilibrium problems in Interfacial Electrochemistry in: A. Wieckowski (Ed.), Interfacial electrochemistry, Theory, Experiment, and Applications, Marcel Dekker, New York, 1999.

[66] M.E.J. Newman, G. T. Barkema, *Monte Carlo Method in statistical physics*. Clarenton –Press Oxford, 1999.

[67] H. B. Callen, *Thermodynamics and an Introduction to Thermostatistics*. John Wiley and Sons, 1985.

[68] S. M . Foiles, M. I . Baskes and M.S. Daw, Phys. Rev. B 1986, 33, 7983